Development of Composite Sponge Scaffolds Based on Carrageenan (CRG) and Cerium Oxide Nanoparticles (CeO2 NPs) for Hemostat Applications

Kimia Alizadeh , Yasaman Dezvare , Shirin Kamyab , Jhaleh Amirian * , Agnese Brangule , Dace Bandere

Posted Date: 31 July 2023

doi: 10.20944/preprints202307.2085.v1

Keywords: Keywords Carrageenan (CRG); Cerium Oxide (CeO2); Nanoparticles (NPs); Composite; antibacterial properties; hemostatic effect

Article

Development of Composite Sponge Scaffolds Based on Carrageenan (CRG) and Cerium Oxide Nanoparticles (CeO_2 NPs) for Hemostat Applications

Kimia Alizadeh [1], Yasaman Dezvare [1], Shirin Kamyab [1], Jhaleh Amirian [2,3,*], Agnese Brangule [2,3,*] and Dace Bandere [2,3]

[1] Department of Life Science, Faculty of New Science and Technology, University of Tehran, North Kargar Street, Tehran, Iran; alizadehn38@gmail.com (K.A.); yasidezi@gmail.com (Y.D.); shirin.kmb@gmail.com (S.K.)

[2] Department of Pharmaceutical Chemistry, Riga Stradins University, Dzirciema 16, LV-1007 Riga, Latvia); dace.bandere@rsu.lv (D.B.)

[3] Baltic Biomaterials Centre of Excellence, Headquarters at Riga Technical University, LV-1658 Riga, Latvia

* Correspondence: jalehamirian@gmail.com and jhaleh.amirian@rsu.lv (J.A.); agnese.brangule@rsu.lv (A.B.)

Abstract: In this study, a novel absorbable hemostatic agent was developed using carrageenan (CRG) as a natural polymer and cerium oxide nanoparticles (CeO_2 NPs). CRG-CeO_2-0.5 and CRG-CeO_2-1 composites were prepared by compositing CRG and CeO_2 at a weight ratio of 200:1 and 100:1, respectively. Physio-chemical and structural properties of these compounds were studied and compared with pristine CRG. Upon incorporation of CeO_2 nanoparticles into the CRG matrix, significant reductions in hydrogel degradation were observed. In addition, it was noted that CRG-CeO_2 exhibited better antibacterial and hemostatic properties than CRG hydrogel without CeO_2.The biocompatibility of the materials was tested using the NIH 3T3 cell line and all samples were found to be nontoxic. Particularly, CRG-CeO_2-1 demonstrated superior hemostatic effects, biocompatibility, and a lower degradation rate since more CeO_2 Nps were present in the CRG matrix. Therefore, CRG-CeO2-1 has the potential to be used as a hemostatic agent and wound dressing.

Keywords carrageenan (CRG); cerium oxide (CeO_2); nanoparticles (NPs); composite; antibacterial properties; hemostatic effect

1. Introduction

Prehospital trauma deaths are largely caused by uncontrolled hemorrhage, whether it occurs in combat or in civilian settings. When such situations arise, materials that stop bleeding and dressings that enhance wound healing are required. Studies have shown that the application of hemostatic dressings can reduce mortality rates and speed up wound healing. Besides their capability to stop bleeding rapidly, they were also capable of protecting against infection. Various materials have been reported to possess favorable characteristics in bleeding management. A variety of hemostatic materials are commercially available, including zeolite powder (ZLP)[1], silica[2], montmorillonite[2], kaolin[3], oxidized cellulose[4], collagen[5], gelatin[6, 7], chitosan[8, 9], silk fibroin[10], calcium alginate[8], fibrin[11], starch[12], peptides[13], polyethylene glycol[14], cyanoacrylate[15], and so on. Although these materials are hemostatic, they also have several limitations, including being expensive, having limited hemostatic or antibacterial effects, and being poorly biodegradable. Therefore, the development of safe and effective new hemostatic materials is essential to overcoming the disadvantages discussed above[16]. Recently, there has been increasing interest in hydrogels made from natural biopolymers, in particular polysaccharides, since they are biodegradable, compatible with living organisms, renewable, and safe[17]. They comprise a three-dimensional (3D) structure that holds a high-water content, thus providing a suitable moist

 doi:10.20944/preprints202307.2085.v1

environment for wound healing [18, 19]. Carrageenan is a polysaccharide derived from red marine algae known as Rhodophyta[20]. It contains long linear chains of D-galactose and D-anhydrogalactose along with anionic sulfate groups ($-OSO_3^-$)[20].

There are many types of antibacterial agents available, including antibiotics, nanoparticels (metal oxides and light-induced antibacterial agents), cationic organic agents, and others, which are applied to combat bacterial infections [21]. Antibiotics are the most commonly used method of treating this condition in clinical practice. However, antibiotic resistance is a concern that must be addressed [21-23]. Therefore, the growing prevalence of antibiotic-resistant bacteria strains in combat trauma wounds poses a growing challenge to clinicians [21]. Thus, the need for other antimicrobial agents to combat antibiotic resistance is apparent [24]. Several emerging fields, including nanomaterials, may be able to offer solutions to this problem, since nanomaterials in some cases can be used to kill bacteria more effectively than conventional antibiotics [24].

Recently, nanomaterials have attracted considerable attention due to their unique properties resulting from higher surface to volume ratios [25]. Nanomaterials possess exceptional capabilities in terms of killing bacteria, compatibility with biological systems, and the ability to promote blood clotting [25]. Currently, cerium oxide nanoparticles (CeO_2 NPs) are considered highly promising for wound healing applications due to their exceptional properties as antioxidants, anti-inflammatory agents, antibacterial, and stimulators of angiogenesis [26]. The incorporation of them into different types of wound dressing, such as films, hydrogels, electrospun mats, sponges and foams, could be considered as an effective way of enhancing the antibacterial effect and controlling infection[27]. Moreover, their compatibility with biological systems and ability to promote clotting make them an ideal choice for treating combat trauma wounds. The combination of hydrogels and nanomaterials may be an effective dressing material for hemostatic and wound healing purposes. It is imperative to develop materials that are able to retain large amounts of water as well as to have antimicrobial properties, blood clotting properties, and biological compatibility.

Therefore, our study aimed to synthesize a novel CRG-CeO_2 composite biomaterial, which was crosslinked using glutaraldehyde. The CRG-CeO_2 composite exhibited suitable physicochemical properties, biocompatibility, hemostatic effect, and antibacterial behavior, suggesting that it could be used as a hemostatic and wound healing agent in the future.

2. Materials and Methods

2.1. Chemical and Reagents

k-carageenan and calcium chloride hydrate were purchased from Sigma Aldrich. Cerium oxide nanopowder was bought from US research nanomaterials. Glutaraldehyde 25% solution in water was supplied from Titrachem. HCl Fuming 37% also was purchased from Merck. All of the chemicals were of analytical grade.

2.2. Methods

In order to prepare carrageenan (CRG) sponges and carrageenan-cerium oxide nanoparticles (CRG-CeO_2) sponges, 0.025 g of carrageenan powder was added to 5 ml of deionized water. Afterwards, the solution was placed into oil bath at 70 °C for 30 minutes until completely dissolved. In subsequent steps, various amounts of CeO_2 NPs in respect to the CRG weight, 0, 0.5, and 1 wt.%, were dispersed in deionized water using a sonicator and separately added to the CRG solutions and stirred in the dark, as shown in Table 1. The pH of the solutions was subsequently adjusted to 3 and 100 µL glutaraldehyde (10% volume ratio) was added to the solution and stirred overnight. In the end, the solutions were poured onto a plate, placed in a -20°C freezer for 24h, and then frozen for 48 hours, as shown in Scheme 1.

Preprints (www.preprints.org) | NOT PEER-REVIEWED | Posted: 31 July 2023 doi:10.20944/preprints202307.2085.v1

Table 1. Summary of sample information, formulations, and concentrations.

Title 1	CRG (wt.%)	CeO_2 NPs(wt.%)
CRG	0.2	0
CRG-CeO2-0.5	0.2	0.005
CRG-CeO2-1	0.2	0.01

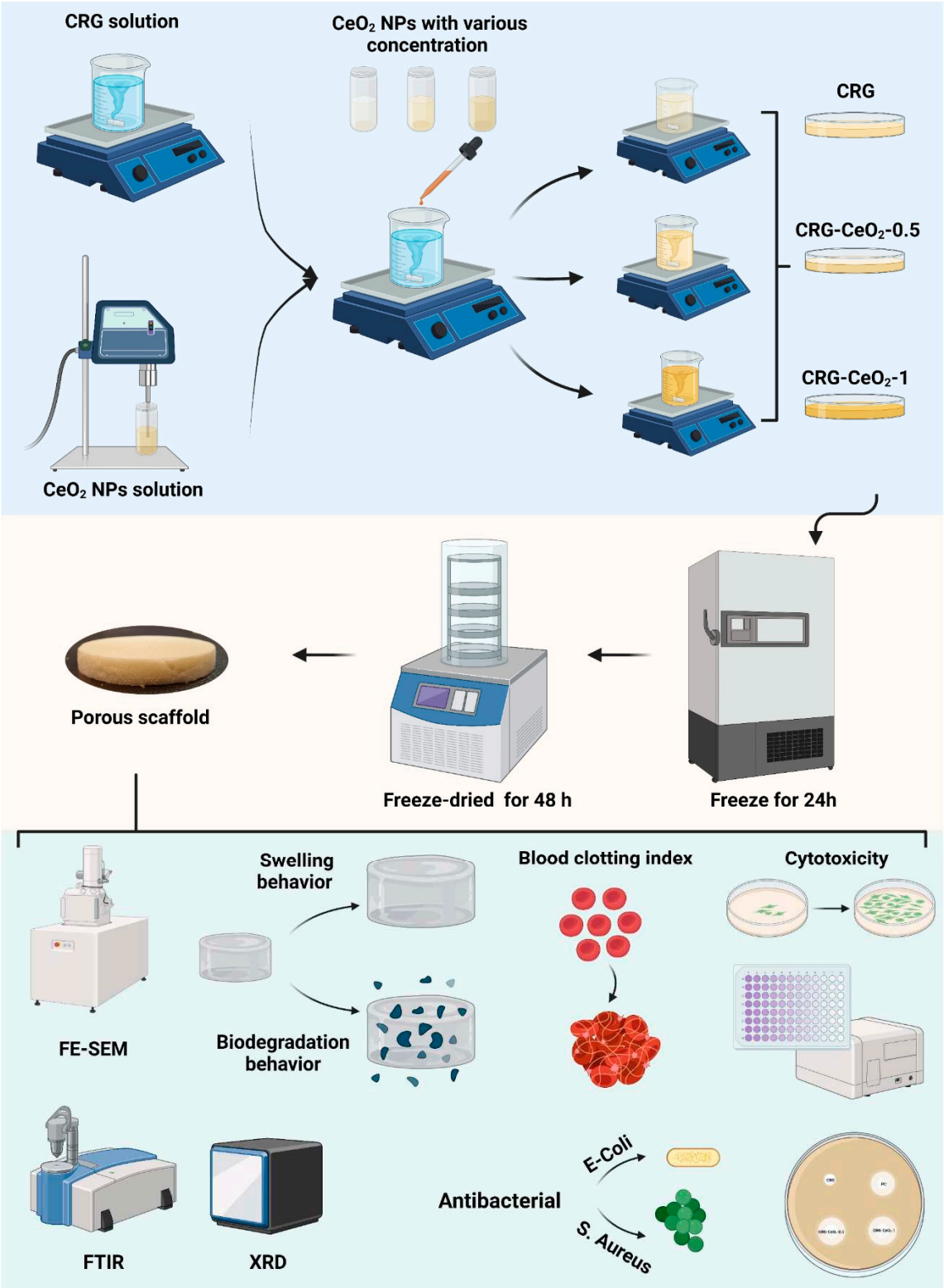

Scheme 1. Schematic representation of the synthesis of CRG, CRG-CeO_2-0.5, and CRG-CeO_2-1 scaffolds with varying percentages of CeO_2 NPs. The Figure created with Biorender.com.

Preprints (www.preprints.org) | NOT PEER-REVIEWED | Posted: 31 July 2023 doi:10.20944/preprints202307.2085.v1

2.3. Characterization

2.3.1. Scanning electron microscopy (SEM)

The surface morphology images of CRG and CRG-CeO_2 composite scaffolds were captured using a scanning electron microscope (FESEM, MIRA3 FEG-SEM, Tescan) operating at 20 kV. Prior to characterizing the samples, they were all sputtered coated with gold.

2.3.2. X-ray diffraction analysis (XRD)

The X-ray diffraction analysis (XRD) was performed using an X-ray spectrometer (Inel, France).

2.3.3. Fourier transform infrared spectroscopy (FTIR)

FT-IR analysis was carried out using a Fourier-transform infrared spectrophotometer (Bruker vector 33, Germany) in the range 400-4000.

2.3.4. Swelling and degradation

The swelling and degradation behaviours of CRG and CRG-CeO_2 composite scaffolds were investigated by immersing them in PBS at 37 °C for designated time intervals. The effect of incorporation of CeO_2 into CRG matrix on the swelling and degradation behaviours of CRG was determined by gravimetric analysis. Initially, the dry weight of CRG and CRG-CeO_2 hydrogels was recorded as W_0. Next, 1 ml of PBS was added to the sample and allowed to incubate at 37 °C. Within designated time intervals (1 h, 2 h, 9 h, and 24 h), the weight of swelling hydrogels was measured until equilibrium was reached. Based on Equation (1), the swelling percentage was determined.

$$Swelling\ ratio\ \% = \frac{Wt - W0}{W0} \times 100, \quad (1)$$

Wt represents the weight of the swollen sample at a predetermined time, while W0 represents the weight of the sample at the beginning of the study.

The degradation of the CRG and CRG-CeO2 composite scaffolds was performed according to ASTM F1635-16 and previous studies, which is widely used in order to assess the degradation of hydrogels. To determine how the hydrogel degraded under PBS at 37 °C, a weight change of the sample was determined in intervals of 1, 3 and 5 days. A degradation percentage was calculated using Equation (2).

$$Degradation\ \% = \frac{W0 - Wt}{W0} \times 100, \quad (2)$$

where Wt represents the weight of the degraded sample at specific time, while W0 represents the weight of the sample at the start.

2.4. Whole-blood clotting index

The determination of the blood clotting index (BCI) was performed according to a method which had been used previously[28]. Recalcified whole blood solution was prepared by adding 8 µL of calcium chloride ($CaCl_2$) to 100 µl of blood at a concentration of 0.2 M. The CRG, the CRG-CeO_2-0.5, and the CRG-CeO_2-1 scaffolds, as well as the gauze, as a positive control, were cut into cylindrical sections (5mm x 8mm) and 50 µL of recalcified whole blood solution was added to them. The samples and the positive control were incubated at various intervals of 30 s, 60 s, 90 s, and 120 s. subsequently, 10 mL of dionized water were carefully added so as not to disturb the clot, and 8 mL of the solution was centrifuged at 3000 rpm for 1 minutes. In the next step, the supernatant was placed in an incubator for one hour. After this time, the absorbance of 2mL of samples and control was determined using a UV-Vis spectrophotometer at wavelength of 540 nm.

 doi:10.20944/preprints202307.2085.v1

2.5. Antibacterial study using disc method

Agar disk diffusion was used to determine the antibacterial activity of the CRG, CRG-CeO_2-O.5, and CRG-CeO_2-1 scaffolds. A study was conducted on two bacteria, including gram-negative Escherichia coli (E. coli, ATCC 9637) and gram-positive Staphylococcus aureus (S. aureus, ATCC 12600). As a first step, 14 grams of nutrient agar (QUELAB) were suspended in 500 ml deionized water and stirred for 15 minutes to obtain a medium culture. Following this, the agar solution was autoclaved for two hours at 121°C. Upon completion of this procedure, the solution was poured into a 10 cm Petri dish. Following solidification, the fresh cultures of the bacteria E.coli and S.aureus were smeared evenly on the gar medium using sterile swabs. CRG, CRG-CeO_2-0.5, and CRG-CeO_2-1 samples were placed aseptically on the agar surface and incubated for 24 hours at 37 °C. The inhibition zones for each sample, if present, were determined and documented after incubation time. As a positive control, vancomycin antibiotic discs (30mg, Padtan Teb company) were used.

2.6. Cytotoxicity study

NIH-3T3 cells were obtained from the National Cell Bank of Iran (NCBI, Tehran, Iran). A RPMI 1640 medium (Gibco, Darmstadt, Germany) supplemented with 10% Fetal Bovine Serum (FBS) and 100 IU per milliliter streptomycin (Gibco, Darmstadt, Germany) were used for cell cultivation.

MTT assay was conducted to determine the viability of cells on the CRG, CRG-CeO_2-0.5 and CRG-CeO_2-1 scaffolds. A minimum of three replications were conducted for each type of sample. Following previous studies[29], the samples were sterilized by soaking in 70% ethanol for 60 minutes and then being washed three times in PBS. A hydrogel extract was obtained by immersing the sterilized samples in 200µl of extract of scaffold in RPMI-1640 culture medium. NIH 3T3 fibroblast cells were seeded in a 96-well plate at a density of 1×10^4 per well. Seed cells were treated for one and three days with extracted medium derived from sterilized hydrogel, RPMI-1640 medium containing 10% FBS. 10 µL of MTT (Bio Idea Co, Iran, with a concentration of 5 mg/mL) was added to the wells after 1, and 3 days, followed by an incubation period of 4 hours at 37 °C. Afterwards, the solutions were removed from the wells, and 100 µL DMSO was added to each well, allowing the crystals to dissolve for one hour. The absorbance of the solution was determined at 570 nanometers with plate reader.

3. Results and discussion

3.1. Nano- and micro- structure and materials properties of the sponges

Figure 1 shows SEM images of freeze-dried CRG, CRG-CeO_2-0.5 and CRG-CeO_2-1 scaffolds. According to low magnification images, all samples appear to be connected and well structured. Additionally, high magnification images of both CRG-CeO_2 composite scaffolds indicate that CeO_2 NPs were well distributed within CRG hydrogels. Depending on the type of sample, the pore size range varied between 40 and 200 µm. This Figure illustrates that pristine carrageenan hydrogel has pores ranging from 60 to190 µm with an average size of 135.69 ± 29.3 µm. It should be noted, however, that the addition of 0.5% and 1% CeO_2 NPs significantly reduced the average pore diameter compared to CRG scaffold. As it can be seen, the addition of 0.5% and 1% CeO_2 NPs significantly reduced the average pore diameter of the CRG-CeO_2-0.5 and CRG-CeO_2-1 composite scaffolds, respectively to 103.02 ± 30.04 µm and 60.5±12.8 µm compared to the pristine CRG. It is attributed to the electrostatic interaction between negatively charged CRG polysaccharide and positively charged CeO_2 NPs, which is consistent with previous findings[1, 2]. By increasing CeO_2 NPs from 0.5 to 1%, the hydrogel became more compact and pores became smaller. Furthermore, CeO_2 NPs may function as crosslinking agents, so altering the amount of CeO_2 NPs can alter the degree of crosslinking[3]. Eventually, this interferes with the growth of the ice crystals during the freezing stage, leading to the result of a reduced pore size on the scaffolds when they are frozen.

Preprints (www.preprints.org) | NOT PEER-REVIEWED | Posted: 31 July 2023 doi:10.20944/preprints202307.2085.v1

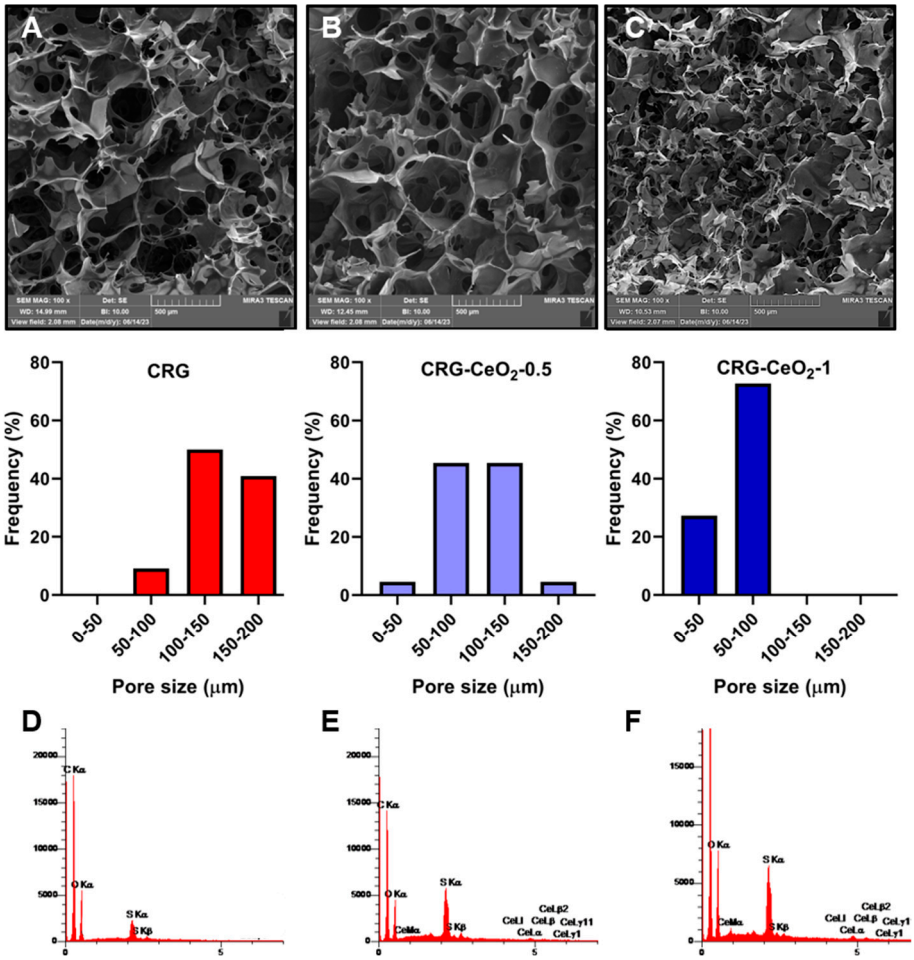

Figure 1. SEM images of the (A) CRG, (B) CRG-CeO_2-0.5, (C) CRG-CeO_2-1 scaffolds and their representative pore size distribution analyzed by imageJ, and EDS profile of (D) CRG, (E) CRG-CeO_2-0.5, and (F) CRG-CeO_2-1 scaffolds.

As shown in Figure 1(D, E, F), the energy-dispersive X-ray spectroscopy (ESD) analysis reveals the presence of C, O, S, and C, O, S, Ce elements in CRG and both CRG-CeO_2 composite hydrogels, respectively. Figure 2. Shown the EDS mapping in both CRG-CeO_2-0.5 and CRG-CeO_2-1 sccafolds. According to the EDS mapping was performed for both of the CRG-CeO_2-0.5 and CRG-CeO_2-1 composite hydrogels, CeO_2 NPs were distributed evenly throughout them.

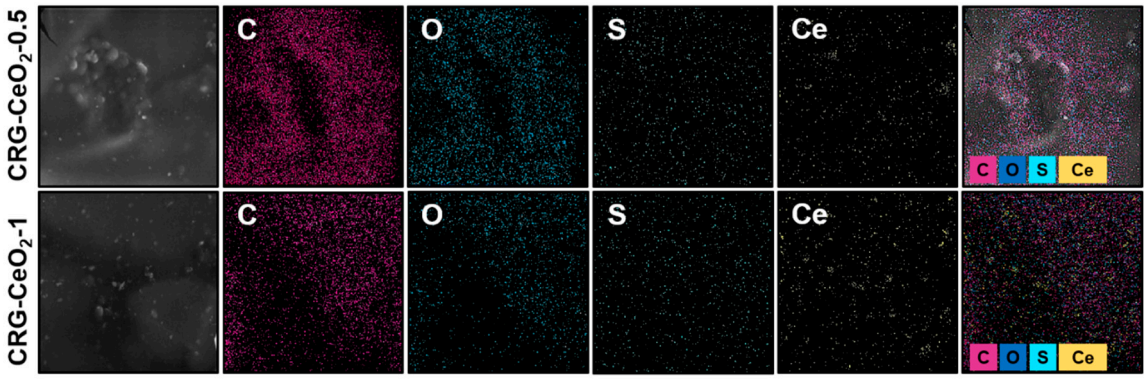

Figure 2. An SEM image and EDX-elemental mapping of CRG-CeO2-0.5 and CRG-CeO2-1 nanostructures showing C (purple), O (blue), S (green) and Ce (yellow).

A FTIR spectroscopy analysis was performed to examine the chemical interaction between CRG and CeO_2 NPs as well as their chemical functionality. Figure 3C shows the FTIR spectrum of CRG,

Preprints (www.preprints.org) | NOT PEER-REVIEWED | Posted: 31 July 2023 doi:10.20944/preprints202307.2085.v1

CRG-CeO_2-0.5, and CRG-CeO_2-1 scaffolds. It can be seen that scaffolds contains CRG exhibit a board band in the 3200-3400 region due to stretching vibrations within O-H groups and hydrogen bonds.[30, 31] Based on the Figure 3D, it is apparent that the peak at 3200 to 3600 cm of width becomes a boundary and intensifies, which is attributed to the formation of both intramolecular and intermolecular hydrogen bonds[31]. Furthermore, two peaks at 2959 and 2850 cm-1 were observed, which are related to the C-H Stretching Bands[32, 33]. Moreover, ester sulfate O=S=O symmetric vibrations occur at 1220 cm^{-1}, -O-SO_3 stretching vibrations occur at D-galactose-4-sulfate (G4S) at 844 cm^{-1}, and D-galactose-2-sulfate (DA2S) at 801 cm^{-1}, respectively[34-37]. All samples containing carrageenan, CRG, CRG-CeO_2-0.5, and CRG-CeO_2-1, exhibited these peaks[34-37]. Moreover, changes in the 1090, 934 cm−1 regions would result in vibrations in the CC, COC, and OH groups in carrageenan structure. There will also be demonstrations of the formation of hydrogen bonds between CeO_2 NPs and CRG, as well as glutaraldehyde crosslinking[38]. In accordance with previous studies, the band at 848 cm^{-1} is associated with a metal-oxygen bond. It is apparent from the results that the addition of CeO_2 NPs intensified peaks at 1066 cm^{-1} and 860 cm^{-1} due to the stretching vibration of Ce-O as well, which is specific to CeO_2[31].

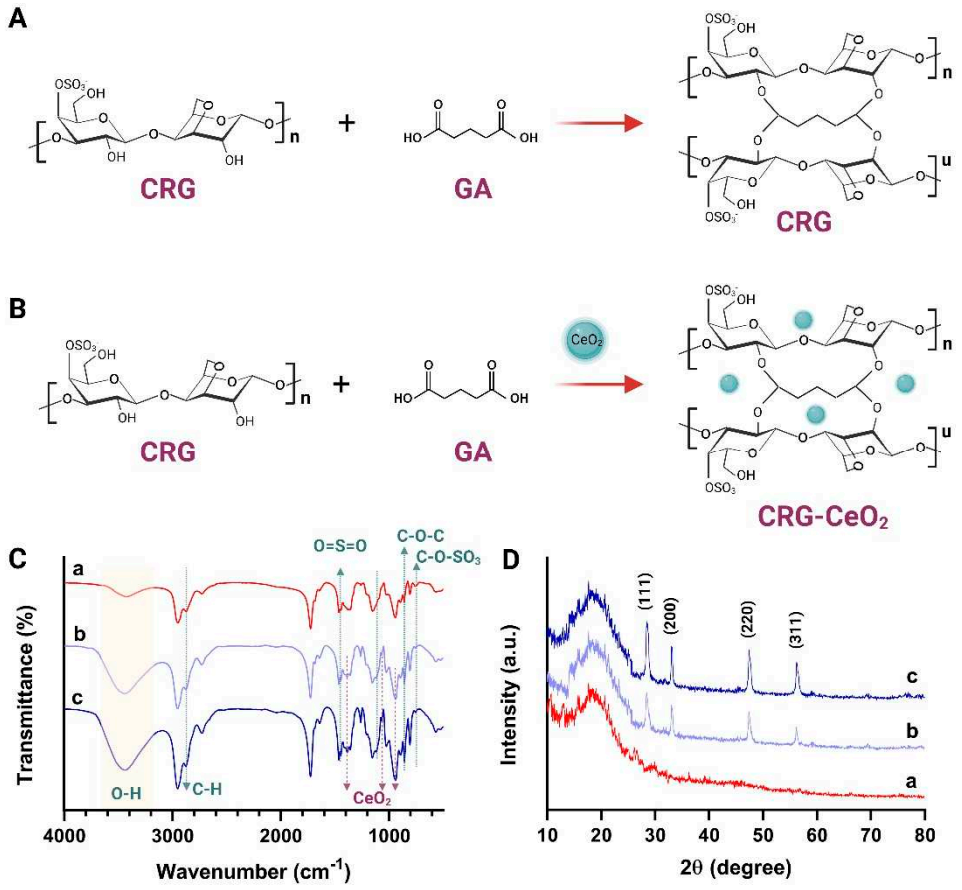

Figure 3. A, B) Schematic of the CRG and CRG-CeO2 scaffolds and their cross-linking with glutaraldehyde, (C) FT-IR, and (D) XRD spectra of a) CRG, b) CRG-CeO2-0.5, and c) CRG-CeO2-0.5.

XRD was used to determine the crystallinity and phase composition of all CRG, CRG-CeO_2-0.5, and CRG-CeO_2-1. Figure 3D illustrates a broad peak in the CRG, a sample without CeO_2 nanoparticles, indicating amorphous carrageenan structures. The introduction of CeO_2 NPs into the κ-carrageenan matrix resulted in the appearance of crystalline peaks at 2θ of 28.4, 33.1˚, 47.4˚ and 56.2˚ specified to (111), (200), (220) and (311) crystallographic plain, respectively[39, 40].

Preprints (www.preprints.org) | NOT PEER-REVIEWED | Posted: 31 July 2023 doi:10.20944/preprints202307.2085.v1

3.2. Swelling and degradation

Figure 4A illustrates the dynamic swelling behavior of CRG and CRG-CeO_2 scaffolds in PBS. The weight of all samples increased within the first few hours of immersion. The weight then started to decrease and then started to level off after a certain period of time. It can be seen that incorporating CeO_2 into CRG results in a decrease in swelling behavior when compared to neat CRG. This decrease in swelling behavior is attributed to the increased cross-linking density of the polymer matrix, due to the incorporation of CeO_2 NPs. This improved cross-linking leads to a more rigid polymer network with fewer voids, resulting in a decrease in swelling behavior. SEM images, Figure 1, illustrates that CRG-CeO_2-1 has a more compact structure with a smaller pore size as compared to CRG-CeO_2-0.5 and CRG hydrogels. Thus, their initial amounts of PBS were reduced in total, which was in accordance with the swelling capability study shown in Figure 4. Earlier studies reported that swelling behavior differed depending on the shape of the porous structure, as well as the type of crosslinking applied using inorganic compounds. There is good agreement between the results of our study and those reported in previous literatures.

Comparatively to CRG, CRG-CeO_2-0.5 and CRG-CeO_2-1 exhibit a lower degradation rate and weight loss value. This can also be attributed to the fact that the presence of more crosslinks in the hydrogel decreases the molecular weights between these crosslinks. Thus, this results in a reduction of the free volume between macromolecular chains, which in turn allows water molecules to penetrate the chain[41]. After five days of incubation, the CRG-CeO_2-1 hydrogels lost 20% of their original weight, which is about 50% less than the weight loss associated with the neat CRG scaffold after five days. The incorporation of CeO_2 NPs into CRG hydrogels with an increasing amount from 0.5 to 1 is attributed to the increased crosslinking density, as well as a decrease in loss weight during incubation.

Hydrogel-based wound dressings are a promising candidate for wound dressing, as they provide moist conditions that speed up the healing process. To facilitate the production of new ECM on the skin, scaffolds should be capable of absorbing between 100 and 800 times their dry weight in water. Such a scaffold should also be able to maintain its shape and structural integrity in the presence of moisture, providing an effective substrate for cell adhesion and growth. The polysaccharides such as carrageenan[42], chitosan[43], pectin[44], etc., bind strongly to water, resulting in easy diffusion of encapsulated therapeutics from them. This results in a low loading capacity and a rapid release rate[45]. To address this issue, inorganic compounds are used to crosslink polysaccharides to reduce their permeability.

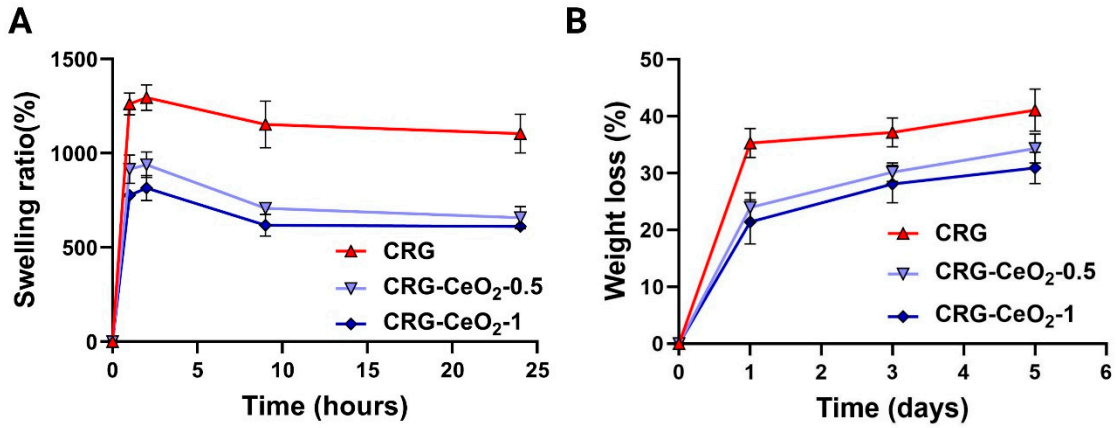

Figure 4. (A) the swelling behavoir, and (B) the in vitro degradation rate of CRG, CRG-CeO_2-0.5 and CRG-CeO_2-1 in PBS at 37 °C.

Preprints (www.preprints.org) | NOT PEER-REVIEWED | Posted: 31 July 2023 doi:10.20944/preprints202307.2085.v1

3.2. In vitro blood clotting evaluation

The blood-clotting capability of materials was assessed using a dynamic whole-blood clotting test, where a solution with a higher absorbance value indicates a slower clotting rate. As a control group, gauze was utilized as a traditional hemostatic agent. In comparison to Gauze, all samples, including CRG, CRG-CeO_2-0.5, and CRG-CeO_2-1, displayed a lower BCI. The CRG-CeO_2-0.5 and CRG-CeO_2-1, however, demonstrated lower BCI values than the CRG, indicating that they have greater hemostatic properties than the CRG. Accordingly, the introduction of CeO_2 into the CRG matrix resulted in a lower BCI rate and an improved clotting index rate in comparison to neat CRG. All samples and controls have shown a downward trend in BCI as the incubating time is extended from 30 s to 120 s. The combination of all factors, including their highly porous structure, swelling properties, rapid blood adsorption, and excellent in vitro blood clotting effect, makes them ideal hemostatic materials.

Currently, CRG is used widely as wound dressings due to its ability to absorb pseudo-extracellular fluid[46]. On the hand, previous studies have shown that negatively charged surfaces in CRG can activate factor XII, initiating the intrinsic coagulation pathway[46]. Studies on mice showed that unmodified CRG had hemostatic properties comparable to Gelfoam (commercial hemostatic agents[46]. The poor mechanical strength of this product makes it difficult to disintegrate after swelling and unable to carry body fluids[46]. Crosslinking the CRG with GA and incorporating CeO_2 NPs into the CRG resulted in improved stability, making the CRG particularly suitable for hemostatic applications. The porous and three-dimensional architecture of the scaffold, as well as the coagulation capability of both CRG and CeO_2 NPs, allow it to absorb and retain blood as well as prevent bleeding. Meanwhile, CRG contain high levels of hydroxyl groups, thus making them hydrophilic biomaterials that may be helpful in surface wetting and adhesion and consequently control bleeding[47].

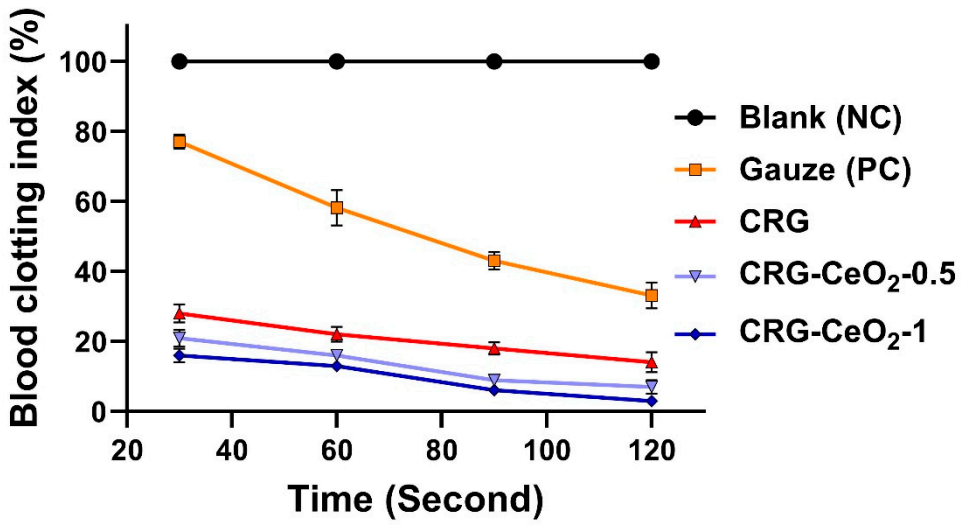

Figure 5. An evaluation of hemostatic capacity for CRG, CRG-CeO_2-0.5, and CRG-CeO_2-1 by comparing the results with a control (Gaze) and a negative control (Blank).

3.3. Antibacterial activity

Antibacterial properties of the composite scaffolds were investigated against S. aureus and E. coli. The Figure 6 shows the antibacterial response of CRG hydrogel with and without CeO_2 NPs after 24 hours of incubation with E. coli bacteria and S. aureus. Observations indicate that both CRG-CeO_2-0.5 and CRG-CeO_2-1 demonstrate antibacterial properties, whereas CRG does not show antibacterial

Preprints (www.preprints.org) | NOT PEER-REVIEWED | Posted: 31 July 2023 doi:10.20944/preprints202307.2085.v1

properties. According to our findings, CRG-CeO_2 hydrogels containing a higher concentration of CeO_2 NPs demonstrated greater activity than hydrogels containing a lower concentration of CeO_2.

The mechanism can be explained by the fact that positively charged NPs were adsorbed onto the membranes of negatively charged Gram-positive and Gram-negative bacteria as a result of electrostatic interactions. In this way, CeO_2 nanoparticles remain on the surface of bacteria for a long time rather than penetrating their membranes, resulting in the blockage of the membranes of bacteria. Following this, NPs may have a detrimental effect on the viscosity of the membrane, impair the specific ionic pumps, and cause a significant disruption in the transport exchange between the bacterial cell and the solution[48]. As a second consideration, CeO_2 NPs may be capable of attacking proteins after it binds to the outer membrane of a bacterial cell [48, 49]. Moreover, the released cerium ions could disrupt electron flow and respiration by bacteria, react with thiol groups (-SH), or be absorbed by transporters and/or porins, thereby preventing the transport of nutrients to the bacteria. Studies demonstrate that CeO_2 NPs can physically damage bacterial membranes, especially Gram-positive bacteria, due to its irregular structure[48, 50].

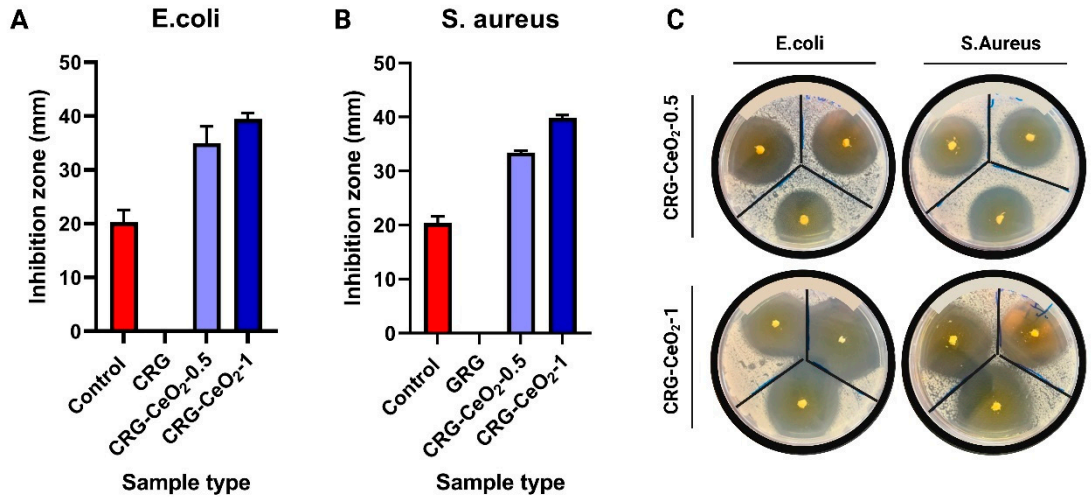

Figure 6. Efficacy of CRG, CRG-CeO_2-0.5, and CRG-CeO_2-1 as antibacterial agents against A) E. coli and B) S. aureus, and C) representative antibacterial properties picture of CRG-CeO_2-0.5 and CRG-CeO_2-1 against E-coli and S-aureus.

3.3. Cell study and cytotoxicity

An evaluation of the cytotoxicity of scaffolds made from CRG, CRG-CeO_2-0.5, and CRG-CeO_2-1 was conducted with the NIH 3T3 cell line. NIH 3T3 cells seeded in 96 well plates were treated with an extracted solution derived from the scaffolds, separately. As shown in Figure 6, all samples exhibited viability greater than 85%, which indicates that the materials are biocompatible. Compared with the CRG scaffold, scaffolds containing CeO_2 NPs, CRG-CeO_2-0.5, and CRG-CeO_2-1, demonstrated a higher degree of cell viability, which is in line with previous studies[39, 51]. CeO_2 NPs were released into the culture medium after 24 hours and 72 hours, leading to an increase in metabolic rate and decreased production of reactive oxygen species (ROS)[39, 52]. However, CRG-CeO_2-1 scaffolds showed an insignificant loss of cell viability on day 3, possibly due to the overexpression of pro-inflammatory factors that may affect cellular function[40].

Preprints (www.preprints.org) | NOT PEER-REVIEWED | Posted: 31 July 2023 doi:10.20944/preprints202307.2085.v1

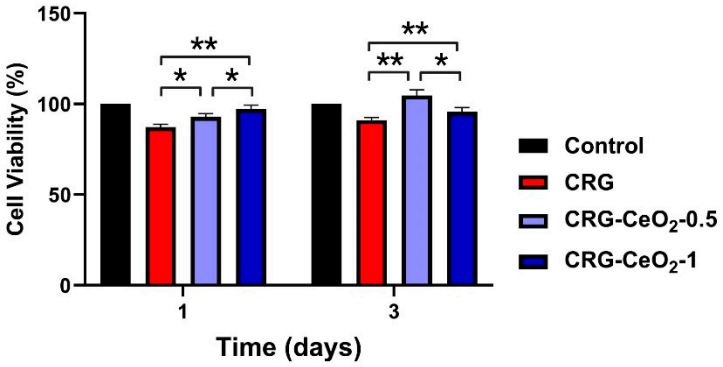

Figure 7. *In vitro* cytotoxicity of CRG, CRG-CeO_2-0.5, and CRG-CeO_2-1 scaffolds with the hNIH 3T3.

5. Conclusions

In this study, we produced CRG and CRG-CeO_2 scaffolds by freeze-drying and crosslinking them with glutaraldehyde. SEM micrographs showed interconnected pores with pore size of around 136, 103, and 60 for CRG and CRG-CeO_2-0.5 and CRG-CeO_2-1, respectively, indicating a more compact structure after incorporating CeO_2 NPs into CRG. Incorporating CeO_2 NPs into CRG matrix enhanced hemostatic performance, as demonstrated by the BCI. The BCI test indicated CRG-CeO_2-0.5 and CRG-CeO_2-1 scaffolds have hemostatic activity comparable to CRG and Gauze (the conventional hemostat in use in hospitals). There is evidence that CeO_2 NPs enhance antibacterial activity in CRG; however, CeO2 concentration influences pore size, degradation, and swelling behaviors. The *in vitro* results also revealed that both CRG-CeO_2-0.5 and CRG-CeO_2-1 showed high cell viability and nontoxic behavior compared to the results obtained with CRG and control samples. According to these findings, incorporation of CeO_2 into CRG hydrogel could lead to the development of hemostatic agents that are antibacterial in nature.

Author Contributions: For research articles with several authors, a short paragraph specifying their individual contributions must be provided. The following statements should be used "Conceptualization, K.A., and J.A.; methodology, K.A., Y.D, .S.K.; software, J.A.; validation, J.A.; formal analysis, K.A., Y.D, .S.K.; investigation, K.A. and J.A.; resources, J.A., A.B., and D.B.; data curation, J.A.; writing—original draft preparation, K.A.; writing—review and editing, J.A.; visualization, J.A.; supervision, J.A, A.B., and D.B.; project administration, J.A., A.B., and D.B.; funding acquisition, J.A., A.B., and D.B.. All authors have read and agreed to the published version of the manuscript." Please turn to the CRediT taxonomy for the term explanation. Authorship must be limited to those who have contributed substantially to the work reported.

Funding: This project has received funding from the European Union's Horizon 2020 research and innovation programme under the grant agreement No 857287.

Data Availability Statement: Not Applicable.

Acknowledgments: Authors acknowledge funding from the European Union's Horizon 2020 research and innovation programme under the Grant Agreement No. 857287 (BBCE). .

Conflicts of Interest: The authors declare no conflict of interest.

References

1. Edwards, J.V., N.T. Prevost, and M.S. Cintron *A Comparison of Hemostatic Activities of Zeolite-Based Formulary Finishes on Cotton Dressings*. Journal of Functional Biomaterials, 2023. **14**, DOI: 10.3390/jfb14050255.
2. Liu, C., et al., *Mussel-inspired degradable antibacterial polydopamine/silica nanoparticle for rapid hemostasis.* Biomaterials, 2018. **179**: p. 83-95.
3. Kondapalli, S.S., et al., *Use of Kaolin-impregnated Gauze for Improvement of Intraoperative Hemostasis and Postoperative Wound Healing in Bslepharoplasty.* J Clin Aesthet Dermatol, 2016. **9**(6): p. 51-5.
4. Zhang, S., et al., *Oxidized cellulose-based hemostatic materials.* Carbohydrate Polymers, 2020. **230**: p. 115585.
5. Kim, H.-H., et al., *Hemostatic efficacy of a flowable collagen-thrombin matrix during coronary artery bypass grafting: a double-blind randomized controlled trial.* Journal of Cardiothoracic Surgery, 2023. **18**(1): p. 193.

6. Mohamed, E., et al., *Superior Hemostatic and Wound-Healing Properties of Gel and Sponge Forms of Nonoxidized Cellulose Nanofibers: In Vitro and In Vivo Studies.* Macromolecular Bioscience, 2022. **22**(10): p. 2200222.
7. Amirian, J., et al., *Gelatin Based Hydrogels for Tissue Engineering and Drug Delivery Applications.* Nanohybrids Future Mater. Biomed. Appl, 2021. **87**: p. 244-270.
8. Hattori, H., et al., *Hemostasis for Severe Hemorrhage with Photocrosslinkable Chitosan Hydrogel and Calcium Alginate.* Annals of Biomedical Engineering, 2010. **38**(12): p. 3724-3732.
9. Fan, P., et al. *Chitosan-Based Hemostatic Hydrogels: The Concept, Mechanism, Application, and Prospects*. Molecules, 2023. **28**, DOI: 10.3390/molecules28031473.
10. Amirian, J., et al., *Versatile Potential of Photo-Cross-Linkable Silk Fibroin: Roadmap from Chemical Processing Toward Regenerative Medicine and Biofabrication Applications.* Biomacromolecules, 2023. **24**(7): p. 2957-2981.
11. Sundaram, M.N., et al., *Bioadhesive, Hemostatic, and Antibacterial in Situ Chitin–Fibrin Nanocomposite Gel for Controlling Bleeding and Preventing Infections at Mediastinum.* ACS Sustainable Chemistry & Engineering, 2018. **6**(6): p. 7826-7840.
12. Zheng, C., et al., *Study on hemostatic effect and mechanism of starch-based nano-microporous particles.* International Journal of Biological Macromolecules, 2021. **179**: p. 507-518.
13. Ghosh, S., et al., *Peptide-based topical agents and intravenous hemostat for rapid hemostasis.* RSC Med Chem, 2020. **11**(10): p. 1100-1111.
14. Serradilla-Martín, M., et al., *Polyethylene glycol-coated haemostatic patch for prevention of clinically relevant postoperative pancreatic fistula after pancreatoduodenectomy: randomized clinical trial.* BJS Open, 2023. **7**(2): p. zrad028.
15. Matsumoto, T., et al., *Cyanoacrylate adhesive and hemostasis.* Arch Surg, 1967. **94**(6): p. 858-60.
16. Chen, X.-J., et al., *An aminocaproic acid-grafted chitosan derivative with superior antibacterial and hemostatic properties for the prevention of secondary bleeding.* Carbohydrate Polymers, 2023. **316**: p. 120988.
17. Baranwal, J., et al., *Biopolymer: A Sustainable Material for Food and Medical Applications.* Polymers (Basel), 2022. **14**(5).
18. Amirian, J., et al., *Examination of In vitro and In vivo biocompatibility of alginate-hyaluronic acid microbeads As a promising method in cell delivery for kidney regeneration.* International Journal of Biological Macromolecules, 2017. **105**: p. 143-153.
19. Amirian, J., et al., *The effect of BMP-2 and VEGF loading of gelatin-pectin-BCP scaffolds to enhance osteoblast proliferation.* Journal of Applied Polymer Science, 2015. **132**(2).
20. Oun, A.A. and J.-W. Rhim, *Carrageenan-based hydrogels and films: Effect of ZnO and CuO nanoparticles on the physical, mechanical, and antimicrobial properties.* Food Hydrocolloids, 2017. **67**: p. 45-53.
21. Kotrange, H. and A. Najda, *Metal and Metal Oxide Nanoparticle as a Novel Antibiotic Carrier for the Direct Delivery of Antibiotics.* 2021. **22**(17).
22. Skadiņš, I., et al. *Antimicrobial and Antibiofilm Properties of Latvian Honey against Causative Agents of Wound Infections*. Antibiotics, 2023. **12**, DOI: 10.3390/antibiotics12050816.
23. Ong, S.-Y., et al., *Development of a chitosan-based wound dressing with improved hemostatic and antimicrobial properties.* Biomaterials, 2008. **29**(32): p. 4323-4332.
24. Gupta, A., et al., *Combatting antibiotic-resistant bacteria using nanomaterials.* Chem Soc Rev, 2019. **48**(2): p. 415-427.
25. Ahmed, H.E., et al. *Green Synthesis of CeO2 Nanoparticles from the Abelmoschus esculentus Extract: Evaluation of Antioxidant, Anticancer, Antibacterial, and Wound-Healing Activities*. Molecules, 2021. **26**, DOI: 10.3390/molecules26154659.
26. Allu, I., et al. *A Brief Review on Cerium Oxide (CeO2NPs)-Based Scaffolds: Recent Advances in Wound Healing Applications*. Micromachines, 2023. **14**, DOI: 10.3390/mi14040865.
27. Andrabi, S.M., et al., *A compositionally synergistic approach for the development of a multifunctional bilayer scaffold with antibacterial property for infected and chronic wounds.* Chemical Engineering Journal, 2021. **423**: p. 130219.
28. Fan, L., et al., *Preparation and characterization of chitosan/gelatin/PVA hydrogel for wound dressings.* Carbohydrate Polymers, 2016. **146**: p. 427-434.
29. Song, M.-J., et al., *Bone morphogenetic protein-2 immobilization on porous PCL-BCP-Col composite scaffolds for bone tissue engineering.* Journal of Applied Polymer Science, 2017. **134**(33): p. 45186.
30. Kim, H., et al. *Heparin-Mimicking Polymer-Based In Vitro Platform Recapitulates In Vivo Muscle Atrophy Phenotypes*. International Journal of Molecular Sciences, 2021. **22**, DOI: 10.3390/ijms22052488.
31. Nourmohammadi, J., et al., *Silk fibroin/kappa-carrageenan composite scaffolds with enhanced biomimetic mineralization for bone regeneration applications.* Mater Sci Eng C Mater Biol Appl, 2017. **76**: p. 951-958.
32. Amirian, J., et al., *Porous BMP-2 immobilized PLGA/Glycol chitosan scaffold with enhanced hydrophilicity, mineralization and osteogenesis.* Materials Letters, 2022. **308**: p. 131140.
33. Amirian, J., et al., *In vitro endothelial differentiation evaluation on polycaprolactone-methoxy polyethylene glycol electrospun membrane and fabrication of multilayered small-diameter hybrid vascular graft.* Journal of Biomaterials Applications, 2020. **34**(10): p. 1395-1408.

34. Zarei Jeliani, Z., et al., *Seasonal variations in growth and phytochemical compounds of cultivated red alga, Hypnea flagelliformis, in southern coastlines of Iran.* Journal of Applied Phycology, 2021. **33**(4): p. 2459-2470.
35. Ghani, N.A.A., et al., *Impact of purification on iota carrageenan as solid polymer electrolyte.* Arabian Journal of Chemistry, 2019. **12**(3): p. 370-376.
36. Tye, Y.Y., et al., *Preparation and characterization of modified and unmodified carrageenan based films.* IOP Conference Series: Materials Science and Engineering, 2018. **368**(1): p. 012020.
37. Zhou, F., et al., *Preparation and Characterization of Biodegradable κ-Carrageenan Based Anti-Bacterial Film Functionalized with Wells-Dawson Polyoxometalate.* Foods, 2022. **11**(4).
38. Petrova, V.A., et al., *Biocomposite films based on chitosan and cerium oxide nanoparticles with promising regenerative potential.* International Journal of Biological Macromolecules, 2023. **229**: p. 329-343.
39. Kalantari, K., et al., *Chitosan/PVA hydrogels incorporated with green synthesized cerium oxide nanoparticles for wound healing applications.* European Polymer Journal, 2020. **134**: p. 109853.
40. Augustine, R., et al., *Cerium Oxide Nanoparticle Incorporated Electrospun Poly(3-hydroxybutyrate-co-3-hydroxyvalerate) Membranes for Diabetic Wound Healing Applications.* ACS Biomaterials Science & Engineering, 2020. **6**(1): p. 58-70.
41. Mohammed, A.H., et al., *Effect of crosslinking concentration on properties of 3-(trimethoxysilyl) propyl methacrylate/N-vinyl pyrrolidone gels.* Chem Cent J, 2018. **12**(1): p. 15.
42. Johnson, A., et al., *Therapeutic effects of antibiotics loaded cellulose nanofiber and κ-carrageenan oligosaccharide composite hydrogels for periodontitis treatment.* Scientific Reports, 2020. **10**(1): p. 18037.
43. Amirian, J., et al., *In-situ crosslinked hydrogel based on amidated pectin/oxidized chitosan as potential wound dressing for skin repairing.* Carbohydrate Polymers, 2021. **251**: p. 117005.
44. Amirian, J., et al., *Bone formation of a porous Gelatin-Pectin-biphasic calcium phosphate composite in presence of BMP-2 and VEGF.* International Journal of Biological Macromolecules, 2015. **76**: p. 10-24.
45. Dafe, A., et al., *Investigation of pectin/starch hydrogel as a carrier for oral delivery of probiotic bacteria.* International Journal of Biological Macromolecules, 2017. **97**: p. 536-543.
46. Barba, B.J.D., C. Tranquilan-Aranilla, and L.V. Abad, *Hemostatic potential of natural/synthetic polymer based hydrogels crosslinked by gamma radiation.* Radiation Physics and Chemistry, 2016. **118**: p. 111-113.
47. Salmasi, S.S., et al., *Polysaccharide-based (kappa carrageenan/carboxymethyl chitosan) nanofibrous membrane loaded with antifibrinolytic drug for rapid hemostasis- in vitro and in vivo evaluation.* International Journal of Biological Macromolecules, 2023: p. 125786.
48. Qi, M., et al., *Cerium and Its Oxidant-Based Nanomaterials for Antibacterial Applications: A State-of-the-Art Review.* Frontiers in Materials, 2020. **7**.
49. Liu, Z., et al., *A series of MOF/Ce-based nanozymes with dual enzyme-like activity disrupting biofilms and hindering recolonization of bacteria.* Biomaterials, 2019. **208**: p. 21-31.
50. Arumugam, A., et al., *Synthesis of cerium oxide nanoparticles using Gloriosa superba L. leaf extract and their structural, optical and antibacterial properties.* Materials Science and Engineering: C, 2015. **49**: p. 408-415.
51. Augustine, R., et al., *Cerium Oxide Nanoparticle-Loaded Gelatin Methacryloyl Hydrogel Wound-Healing Patch with Free Radical Scavenging Activity.* ACS Biomaterials Science & Engineering, 2021. **7**(1): p. 279-290.
52. Singh, M.R., S. Patel, and D. Singh, *Chapter 9 - Natural polymer-based hydrogels as scaffolds for tissue engineering*, in *Nanobiomaterials in Soft Tissue Engineering*, A.M. Grumezescu, Editor. 2016, William Andrew Publishing. p. 231-260.